

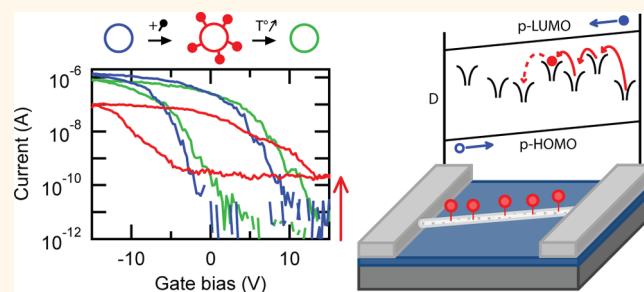
# Graft-Induced Midgap States in Functionalized Carbon Nanotubes

Delphine Bouilly,<sup>†,‡</sup> Jonathan Laflamme Janssen,<sup>†,||</sup> Janie Cabana,<sup>‡</sup> Michel Côté,<sup>†,§</sup> and Richard Martel<sup>\*,‡,§</sup>

<sup>†</sup>Département de Physique, Université de Montréal, C.P. 6128 Succursale Centre-Ville, Montréal, Québec H2C 3J7, Canada, <sup>‡</sup>Département de Chimie, Université de Montréal, C.P. 6128 Succursale Centre-Ville, Montréal, Québec H2C 3J7, Canada, and <sup>§</sup>Regroupement Québécois sur les Matériaux de Pointe (RQMP), Montréal, Québec H2C 3J7, Canada. <sup>‡</sup>Present address: Columbia University, New York, New York 10027, United States. <sup>||</sup>Present address: Université Catholique de Louvain, Louvain-la-Neuve 1348, Belgium.

**ABSTRACT** Covalent addition of functional groups onto carbon nanotubes is known to generate lattice point defects that disrupt the electronic wave function, resulting namely in a reduction of their optical response and electrical conductance. Here, conductance measurements combined with numerical simulations are used to unambiguously identify the presence of graft-induced midgap states in the electronic structure of covalently functionalized semiconducting carbon nanotubes. The main experimental evidence is an increase of the conductance in the OFF-state after covalent addition

of 4-bromophenyl grafts on many single- and double-walled individual nanotubes, the effect of which is fully suppressed after thermodesorption of the adducts. The graft-induced current leakage is thermally activated and can reach several orders of magnitude above its highly insulating pristine-state level. *Ab initio* simulations of various configurations of functionalized nanotubes corroborate the presence of these midgap states and show their localization around the addends. Moreover, the electronic density of these localized states exhibits an extended hydrogenoid profile along the nanotube axis, providing access for long-range coupling between the grafts. We argue that covalent nanotube chemistry is a powerful tool to prepare and control midgap electronic states on nanotubes for enabling further studies of the intriguing properties of interacting 1D localized states.



**KEYWORDS:** carbon nanotubes · covalent functionalization · diazonium salt · 1D defect · midgap states

Electronic devices rely largely on the control of point defects and disorder to tune the properties of semiconducting materials such as charge carrier density, recombination rates and mobility.<sup>1</sup> In low-dimensional materials, the influence of point defects is expected to be even more prevalent due to their large surface-to-bulk ratio and reduced electronic density of states. Various quasi-1D materials have been produced in the past decades, such as carbon nanotubes,<sup>2</sup> graphene nanoribbons<sup>3</sup> and numerous species of nanowires.<sup>4,5</sup> Among them, carbon nanotubes are particularly appropriate to study the influence of defects, as their closed-up tubular structure makes them free of extended edge-type defects such as dangling bonds. Point-defects in carbon nanotubes<sup>6,7</sup> can be generated during growth<sup>8</sup> or induced *a posteriori* by mechanical stress,<sup>9</sup> ion irradiation<sup>10,11</sup> or chemical functionalization of the sidewall.<sup>12,13</sup> Functionalization approaches have been extensively

developed in the past 15 years on nanotubes, as they bear many advantages such as improving their processability<sup>14,15</sup> and tuning their chemical and biological affinity.<sup>16,17</sup> Hence, chemical functionalization offers particularly impressive control and versatility in terms of grafting types.<sup>12,13</sup>

Grafting functional groups onto a nanotube sidewall creates point-like defects that alter the nanotube electronic properties. The disruption is minor for noncovalent binding<sup>18,19</sup> but much more invasive in the case of covalent adducts, which deeply modify the electronic orbitals of the nanotube. Most common covalent grafting reactions, such as hydrogenation,<sup>20,21</sup> halogenation,<sup>22,23</sup> carboxylic addition<sup>24</sup> and aryl radical additions using the well-known diazonium precursor,<sup>25,26</sup> are monovalent additions generating  $sp^3$ -type of defects that strongly disrupt the optical and electrical properties of the nanotube. Loss of optical response has been reported in absorption spectroscopy<sup>27</sup>

\* Address correspondence to r.martel@umontreal.ca.

Received for review November 4, 2014 and accepted February 9, 2015.

Published online February 09, 2015 10.1021/nn506297z

© 2015 American Chemical Society

and resonant Raman spectroscopy has shown that modes associated with the nanotube are reduced in intensity, whereas defect modes are enhanced.<sup>27</sup> Likewise, studies have reported a significant loss of electrical conductance after functionalization,<sup>28–30</sup> even in the case of single-point functionalization.<sup>31</sup> Selectivity with diameter, chirality or electrical type can be observed at low graft density,<sup>28,30,32</sup> which is often considered as a particularly useful route for selecting metallic or semiconducting species in assembling processes.<sup>28,33,34</sup> The selectivity usually disappears at high graft density as the amplitude of the alteration increases.<sup>28,30</sup> Finally, functional groups can generally be removed from the nanotube sidewall by a thermal annealing in a vacuum or inert atmosphere,<sup>25,32,35,36</sup> However, electronic properties are generally not fully restored after defunctionalization, and such residual damage accumulates after successive cycles of functionalization and defunctionalization.<sup>37</sup>

The drastic impact of monovalent additions on the properties of nanotubes can be appreciated through band structure and conjugation considerations. Optical and electrical properties of nanotubes arise from the 1D electronic bands and corresponding Van der Hove singularities associated with the delocalized  $\pi/\pi^*$  orbitals.<sup>38</sup> The introduction of  $sp^3$  point-defects in the structure causes destructive rehybridization,<sup>26</sup> *i.e.*, conversion of previously delocalized  $\pi$ -electrons in localized chemical bonds with the grafts, which strongly perturbs the nanotube electronic bands. Furthermore, this addition breaks the symmetry between the two nonequivalent carbon atoms in the primitive cell of the honeycomb lattice, which is expected to lift the 2-fold valley degeneracy in the nanotube band structure, and generates  $\pi$ -radical species in the carbon lattice.<sup>26</sup> On the opposite, covalent reactions that preserve the symmetry and long-range conjugation of the wave function, such as divalent  $sp^2$ -like grafting with carbene addition reactions, have been found to leave the transport properties of nanotubes mostly unaltered.<sup>39,40</sup> Several theoretical calculations effectively predicted  $sp^3$ -like point defects to disrupt the singularities in the density of states as well as the electrical conductance of nanotubes.<sup>6,41–43</sup> However, despite all the evidence of their dramatic effect on nanotube properties, little is known about the resulting electronic states of  $sp^3$ -functionalized carbon nanotubes and their properties.

In this study, we use electrical transport experiments and density functional theory (DFT) calculations to investigate the electronic states induced by covalent functionalization of carbon nanotubes. Using aryldiazonium salt reactions onto many individual semiconducting single-walled and double-walled carbon nanotubes (SWNTs and DWNTs), our experiments show that monovalent graft addition induces a strong conductance increase in the OFF-state, indicating the presence of midgap electronic states that allow for long-range

charge transport. The effect is reversible after removal of the grafts by thermal annealing, therefore unambiguously linking it to the presence of the adducts. The graft-induced leakage current is thermally activated and can reach several orders of magnitude over the highly insulating OFF-state of pristine nanotubes. *Ab initio* simulations of semiconducting SWNTs functionalized in various configurations of covalent adducts reveal the apparition of graft-induced midgap states, which electronic density profiles are localized on the graft sites and exhibit hydrogenoid-like extensions along the nanotube axis allowing for long-range interaction between graft states. Covalently functionalized semiconducting nanotubes are revealed here as an ideal template for studies on the properties of 1D localized states.

## RESULTS AND DISCUSSION

In order to unambiguously assess the effect of covalent functionalization on electrical properties of carbon nanotubes, it is necessary to measure the electrical response of the same nanotubes with and without the grafts. The protocol to do so is illustrated in Figure 1: carbon nanotubes were individually assembled in devices and their electrical response was acquired in pristine (p), functionalized (f) and defunctionalized (d) states.<sup>44</sup> The devices were fabricated in a field-effect transistor configuration with an individual nanotube as the channel, either using laser ablation SWNTs<sup>45</sup> or CVD-grown DWNTs.<sup>46</sup> Functionalization was performed directly on the devices by immersion in an aqueous solution of 4-bromobenzenediazonium tetrafluoroborate,<sup>44,47</sup> at high concentration to facilitate

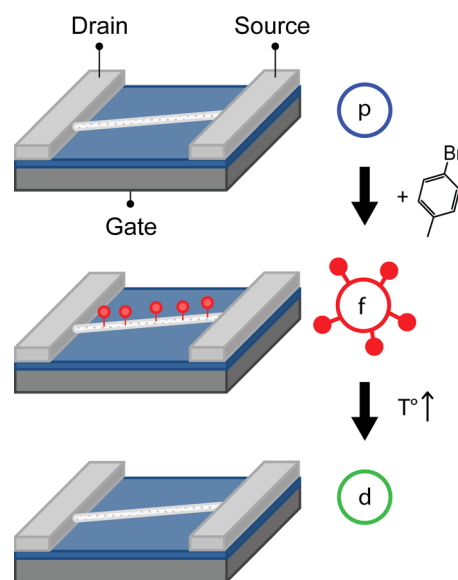


**Figure 1.** Experimental setup and procedures. Carbon nanotubes are organized individually in a field effect transistor configuration with drain, source and gate electrodes. Electrical characteristics are probed in three states: (p) pristine state, *i.e.*, before functionalization, (f) functionalized state after adding 4-bromophenyl-grafts, and (d) defunctionalized state after thermal annealing in a vacuum.

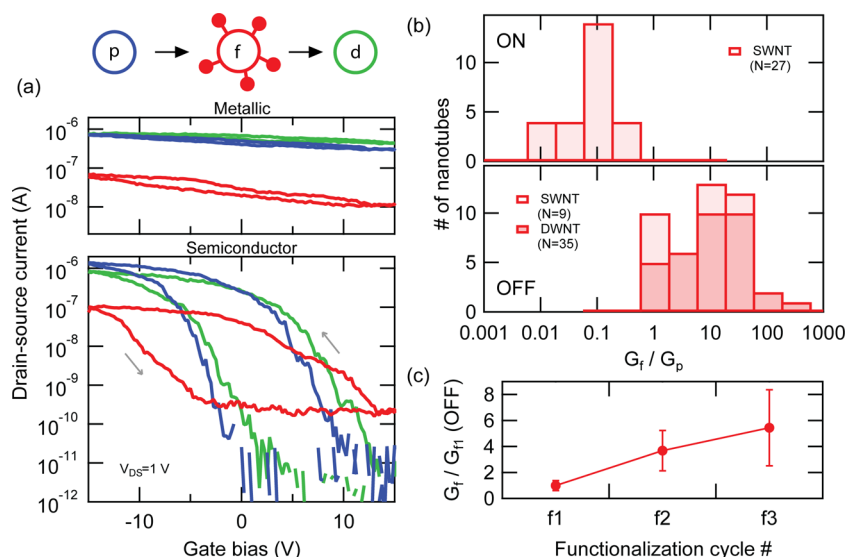


**Figure 2.** Effect of functionalization on both the ON-state and OFF-state conductances of the devices. (a) Typical electrical transfer characteristics of metallic (top) and semiconducting (bottom) SWNTs in pristine (blue), functionalized (red) and defunctionalized (green) states. Gray arrows indicate the direction of gate bias sweep. (b) Distribution of conductance change, *i.e.*, ratio of functionalized over pristine conductance, in ON-state (top) and OFF-state (bottom) for ensembles of nanotubes. (c) Further increase of OFF-state conductance after successive defunctionalization and refunctionalization cycles, averaged over 22 devices and normalized with first functionalized-state.

reaction regardless of nanotube chirality.<sup>28</sup> Removal of the grafts was performed by thermal annealing at 500 °C in a vacuum.<sup>36</sup> Details on device fabrication as well as functionalization/defunctionalization processes are provided below in the Experimental and Numerical Methods section.

The impact of chemical functionalization on the ON- and OFF-state currents of carbon nanotubes was investigated using their device transfer characteristics, obtained by sweeping the gate bias back and forth (from  $-15$  to  $+15$  V) at fixed drain-source bias (here 1 V). Blue traces in Figure 2a show transfer curves from typical metallic (top) and semiconducting (bottom) nanotubes. While the conductance of metallic species is rather independent of gate bias, it is modulated by several orders of magnitude in the case of semiconductors. In the latter, the electrical current switches from a high value at large negative gate bias (ON-state) to a minimum when gate bias is pushed toward positive values (OFF-state). The high ON-state conductance is due to strong field-effect doping by hole carriers, while the conductance in OFF-state drops below noise level due to full depletion of carriers when the gate field aligns the Fermi level within the nanotube band gap. In principle, we would expect to see a second highly conductive regime due to electron doping at large positive gate bias, but this regime is blocked in most SWNTs by charge trapping due to oxygen/water redox reactions in ambient conditions.<sup>48</sup> This regime is however observed in large diameter nanotubes, such as DWNTs (see Figure 3), because of their much smaller band gap. Note that all traces exhibit a strong hysteresis between forward and reverse gate sweep, which is

typical in carbon nanotube devices due to charge traps and ionic movements at the dielectric surface.<sup>49</sup>

The effect of functionalization is presented with the red curves in Figure 2a, measured after covalent bonding of the grafts. Conductances of metallic nanotubes and of semiconducting nanotubes in their ON-state exhibit a marked drop by about 1 order of magnitude, which is consistent with previous studies.<sup>28,30,37,44</sup> However, the OFF-state shows a completely different behavior: the conductance *increases* after addition of the chemical adducts. The increase is strong, with an amplitude reaching at least 2 orders of magnitude above the resolution-limited insulating current of the pristine nanotube. This effect was never reported before, and therefore we performed a quantitative analysis using measurements repeated on a large ensemble of SWNT and DWNT devices. For each, we calculated the  $G_f/G_p$  ratio, *i.e.*, the ratio of functionalized-to-pristine-state conductances, in both ON- and OFF-states. The obtained distributions of  $G_f/G_p$  ratios are presented in Figure 2b and 2c, respectively. In the ON-state, all ratios are inferior to 1, indicating a decrease of conductance, with a distribution centered at 0.1 corresponding to a typical decrease of 1 order of magnitude. In the OFF-state, all SWNT and DWNT devices show a ratio superior or equal to 1, which indicates either an increase of conductance or no measurable change. Devices reporting no detectable effect are in fact those for which both conductance levels, before and after functionalization, lie below the resolution limit. In all other cases, an increase of conductance is observed, which amplitude can reach up to 3 orders of magnitude. Note that

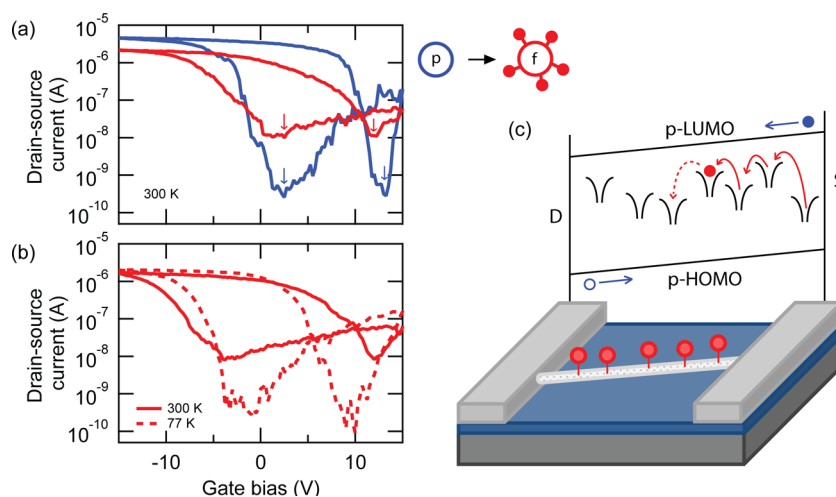


**Figure 3.** DWNTs and transport mechanism. (a) Transfer characteristics of a typical S@S DWNT in pristine and functionalized states at room temperature. Small arrows indicate the threshold (or OFF-state) voltage. (b) Temperature dependence of the functionalized DWNT transfer characteristics, showing thermal activation of the OFF-state conductance. (c) Representation of the proposed mechanism for OFF-state conductance: hopping transport between graft-induced localized gap states.

pristine OFF-state measurements are actually limited by the resolution of the apparatus and so the conductance increase, as calculated here, is a lower bound.

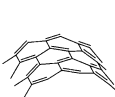
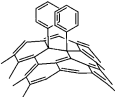


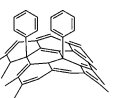
Alterations in ON- and OFF-state conductances are reversible upon removal of the functional groups, as shown by the great similarity between blue and green lines in Figure 2a. The changes in functionalized states are thus conclusively attributed to the presence of the grafts. A cumulative effect upon cycling functionalization and defunctionalization steps is also observed. Figure 2c reports the averaged conductance of 22 devices after consecutive functionalization steps, normalized by averaged conductance in the first functionalized state. Devices were annealed for defunctionalization between each step, and gate bias was fixed at +15 V to probe the OFF-state of semiconducting SWNTs.<sup>37</sup> After each functionalization step, the OFF-state conductance further increases, which is consistent with an accumulation of residual defects induced by the grafting reaction, as reported elsewhere.<sup>37</sup>

The increase of OFF-state conductance after functionalization is definitely surprising. In this regime, semiconducting nanotubes are normally insulators and current is limited by thermal emission over the band gap and tunnelling through the Schottky contacts. Better electrical conduction after the introduction of defects is *a priori* rather counterintuitive. One could argue at this point that the phenomenon is simply caused by a large upshift of the threshold voltage due to charge transfer between the grafts and the nanotube, preventing full carrier depletion in the channel within the probed gate bias range. Such charge transfer is however refuted by both numerical simulations (see Supporting Information) and additional measurements on double-walled carbon nanotubes (DWNTs). Figure 3a presents transfer curves from a typical DWNT composed of two semiconducting

walls (S@S), in pristine (blue) and functionalized (red) states. We previously showed in ref 44 that charge transport in a pristine DWNT occurs through both walls, and that functionalization alters only the properties of the outer wall.<sup>44</sup> The strong conductance modulation in this pristine DWNT (blue curve) indicates that both walls are of semiconducting type.<sup>44</sup> The ambipolar character of the DWNT is visible from the two ON-state branches in the transfer curve, and allows to pinpoint the position of the threshold voltage, *i.e.*, the gate bias corresponding to the lowest conductance. After functionalization (red curve), the OFF-state conductance increases sharply, similarly to the case of SWNTs, but this time we can clearly see that the threshold voltage does not change significantly (forward sweep: stays at 2.5 V; reverse sweep: changes slightly from 13.25 to 12.25 V). There is definitely no indication of strong hole doping here, which refutes the hypothesis of functionalization-induced charge transfer to explain the increase of the OFF-state conductance. Another hypothesis, which is most probable, is that functionalization generates additional midgap states, *i.e.*, electronic states that are comprised in energy within the nanotube band gap. Charge transport through those states would form an additional conductance path leading to a “leakage current” in the OFF-state. In the case of DWNTs, these gap states should be generated only in the outer wall, which would then contribute to the OFF-state current while the inner wall would remain insulating. This hypothesis of graft-induced gap-states leakage current is further tested in the following by a combination of experiments and calculations.

In carbon nanotubes, we know that the electrical current amplitude is mainly controlled by charge transmission at the interface with the metallic electrodes of the contacts.<sup>50</sup> The OFF-state, which is the conductance minimum, corresponds to an electrostatic doping level

TABLE 1. Density Functional Theory (DFT) Simulations<sup>a</sup>

						
		pristine	<i>ortho</i>	<i>meta</i>	<i>para</i> 0°	<i>para</i> 60°
(13,0)	$E_{gap}$ (eV)	0.70	0.42	0.02	0.72	<b>0.48</b>
	$E_{binding}$ (eV)	-	-1.59	-1.08	-2.41	<b>-2.57</b>
(16,0)	$E_{gap}$ (eV)	0.60	0.34	0.02	<b>0.60</b>	0.42
	$E_{binding}$ (eV)	-	-2.16	-1.74	<b>-2.74</b>	-1.83
(17,0)	$E_{gap}$ (eV)	0.56	0.52	0.00	0.28	<b>0.46</b>
	$E_{binding}$ (eV)	-	-1.73	-1.75	-2.44	<b>-2.61</b>

<sup>a</sup> Simulated band gaps ( $E_{gap}$ ) for (13,0), (16,0) and (17,0) nanotubes functionalized with 4-bromophenyl pairs in diverse relative positions, as well as the binding energy ( $E_{binding}$ ) of graft pairs. The most stable configuration is identified with bold fonts.

such that the band bending maximizes the height of the injection barriers. At fixed temperature, the observed increase in the OFF-state conductance can actually be reproduced by a lowering of injection barriers, *i.e.*, an effective reduction of the nanotube band gap. With this understanding of nanotube transport, experimental observations supporting the hypothesis of midgap states due to graft-induced  $sp^3$ -defects can be summarized as follows: First, the rather moderate intensity of the leakage current compared to the band current is compatible with thermally activated transport such as thermal emission or hopping mechanisms, which are typically more resistive than delocalized band transport. The leakage current is indeed activated by temperature, as shown in Figure 3b. In this graph, both traces are from a DWNT in functionalized state measured in a vacuum. The plain line is the response of the functionalized DWNT at room temperature (300 K), which is comparable to that in air, as in Figure 3a. When cooled down at 77 K, the dotted line shows that the leakage current drops down by 2 orders of magnitude, consistent with what is expected in thermal activated transport when the carrier thermal energy decreases.<sup>51</sup> The detailed transport mechanism in this regime is yet unclear and falls outside the scope of this paper.<sup>52</sup> Furthermore, the radical nature of the diazonium chemistry used here currently limits our ability to lower the coverage of addends down to the interesting limit of long-range distances between localized states. It should be noted however that variable range hopping transport was reported by Zhang *et al.* in functionalized graphene using similar 4-nitrophenyl units.<sup>53</sup> In the light of all this and the calculations presented below, we can speculate that OFF-state transport occurs through hopping between graft-induced localized gap states.

Further insights into the microscopic nature of the gap states in functionalized carbon nanotubes were obtained using simulations based on density functional theory (DFT). Semiconducting SWNTs were modeled with and without a grafted 4-bromophenyl pair,

since pair formation is expected on semiconducting nanotubes.<sup>35,54</sup> Different relative positions were tested for the pair, *i.e.*, the *ortho*, *meta* and *para* configurations.<sup>54</sup> Since the *para* configuration is usually more stable,<sup>35,54</sup> it was more thoroughly investigated; *i.e.*, all its possible orientations on a zigzag SWNT were simulated (0° and 60° with respect to the nanotube axis). Semiconducting chiralities (13,0), (16,0) and (17,0) were selected for the calculations, as their respective diameters of 1.03, 1.27 and 1.35 nm are comparable to the average diameter of the SWNTs used in the experimental part of this study (1.3 nm).<sup>45</sup> Table 1 reports the simulated band gap associated with each configuration, as well as the corresponding binding energy of the graft pair. Simulated electronic dispersion and wave function for each configuration can be found in Figures S1 and S2 in the Supporting Information. The simulations show graft-induced states that vary substantially between different grafting configurations. For instance, the *meta* configuration with two free radicals generates deep states in the middle of the nanotube band gap, which are strongly localized as seen from the shape of the wave function (see Figure S2) and the absence of dispersion (see Figure S1). *Ortho* and *para* configurations also generate graft-induced states in the nanotube band gap, although these are more shallow and more hybridized with the nanotube dispersive states. The important conclusion here is that, for all the chiralities simulated, most of the binding configurations generate midgap states, including some of the most stable *para* configurations. In experimental conditions, a distribution of the various grafting configurations should be found on nanotube sidewalls, at least a mixture of the few most stable configurations; hence, gap states are definitely to be expected in the electronic structure of functionalized nanotubes.

Charge transport properties through these midgap states are function of the coupling between them, and hence they are also function of the properties of their wave function. Figure 4 presents the simulated wave

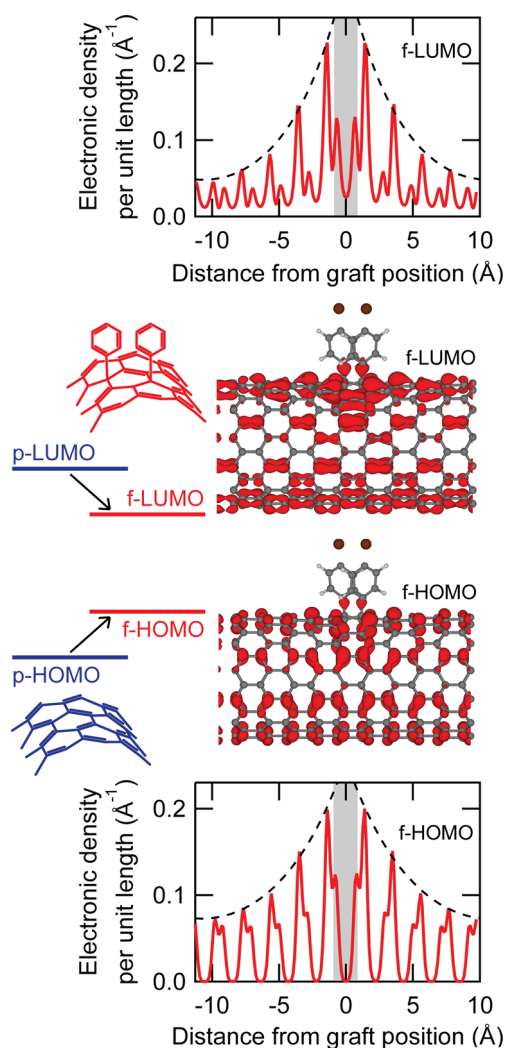


**Figure 4.** Simulated wave function and electronic density. f-HOMO and f-LUMO wave functions for a (13,0) nanotube functionalized with a 4-bromophenyl- pair in its most stable *para* 60° configuration. The corresponding electronic density per unit length along the nanotube axis (red line) is centered at the graft position and decays slowly around it. The envelope is fitted by a periodic hydrogenoid function (dotted line).

function of the f-HOMO and f-LUMO levels as well as the corresponding electronic density per unit length along the nanotube axis for a (13,0) nanotube functionalized in *para* 60° configuration. Both levels correspond to midgap states as their energies are located within the pristine nanotube band gap. They are also strongly associated with the grafts, as the electronic density profile is centered on the grafting site. The corresponding electronic bands (Supporting Information, Figure S1 bottom-left) show significant dispersion, indicative of coupling between the periodically arranged grafts. Indeed, these states show a slow spatial decay, extending several C–C bonds away from the grafting site, suggesting the possibility of graft-to-graft coupling. In order to extract the spatial extent of these midgap states, the envelope

of the simulated electronic density was adjusted by a hydrogenoid or shallow-defect model,<sup>55</sup> including periodic replicas along the nanotube axis to capture effects produced by the periodic boundary conditions inherent to the numerical calculations. The model shows a good agreement with the simulation, as shown by the dotted black line in Figure 4. The obtained effective Bohr radii are  $(11.1 \pm 0.3)$  Å for the HOMO and  $(8.3 \pm 0.2)$  Å for the LUMO, which correspond to the exponential decay rates of the wave function along the nanotube axis.

In the experiment, we report a grafting density of approximately 1%, which corresponds to one graft pair every 16.5, 13.4 and 12.7 Å for the (13,0), (16,0) and (17,0) nanotubes, respectively. Comparison between experiment and simulation should be taken with caution since experimentally grafted tubes are expected to hold a mixture of grafting configurations distributed rather randomly over the length as well as the circumference of the nanotube. A variation of the graft density parameter was unfortunately not possible to explore due to a lack of control over the diazonium salt reaction at low coverage. As discussed by Chevrier *et al.*,<sup>34</sup> the selectivity and radical nature of diazonium coupling compounded with the presence of different nanotube species makes it difficult to precisely control the graft density on individual nanotubes. Nevertheless, considering the similarity of length scale between the spacing of the grafts and the extent of their wave function, one can reasonably expect significant coupling between grafts, allowing for long-range charge transport along the nanotube length.

## CONCLUSIONS

Our work demonstrates the existence of graft-induced localized electronic midgap states in covalently functionalized carbon nanotubes. These states were experimentally revealed by a strong and surprising increase in the OFF-state conductance of the nanotubes after functionalization, which disappeared upon removal of the grafts. Charge transport is found to be mediated by these midgap states, which is supported by temperature-dependent transport measurements and *ab initio* calculations. The latter revealed that the midgap state wave functions are sufficiently extended to allow long-range interaction. In light of this study, functionalized carbon nanotubes appear as a robust template to study one-dimensional transport through localized states. The strong backbone of the nanotube structure combined with the robustness of covalent chemistry allows to prepare high-quality devices in which the conductance of these gap states can be enhanced and detected. One can then take advantage of the huge versatility of chemistry to control the spatial extent and energetic distribution of these midgap states by varying

graft type and density. Alternatively, one could use the thermal transport properties of the states to

investigate temperature-sensitive chemical reactions taking place on the grafts.

## EXPERIMENTAL AND NUMERICAL METHODS

**Nanotube Devices Fabrication.** All nanotube devices for this study were fabricated according to an established protocol presented previously in ref 44. Briefly, standard silicon substrates (100 nm SiO<sub>2</sub>/n<sup>+</sup> Si) were pretreated to enhance nanotube adhesion (piranha treatment + aminosilane (APTS) vapor exposition<sup>56</sup> for SWNTs; RCA treatment for DWNTs). Note for reader: Extreme care should be exerted when manipulating piranha solution in contact with organic compounds. Suspensions of carbon nanotubes were prepared from powder sources (SWNT: laser ablation source,<sup>45</sup> suspension in dimethylformamide (DMF) after reflux in nitric acid (10% per volume, 24 h) and water (2 h); DWNT: chemical vapor deposition source,<sup>46</sup> supernatant extracted from a dispersion in 1,2-dichloroethene (DCE) decanted for 2 weeks), and drops were deposited on the substrates by spin-coating (followed by drops of DCE for cleaner drying in the case of DMF suspensions). The suspension concentration and number of drops were calibrated to optimize the yield of isolated nanotubes on the substrate. When necessary, low-power sonication of the substrates in acetone was used to remove residual amorphous/bundled carbon material. Metallic electrodes were deposited on top of the isolated nanotubes using optical lithography and e-beam metal evaporation (Ti 0.5 nm + Pd 25 nm), so as to pattern channels of 1, 2, or 3 μm. All devices were finally annealed at 500 °C in a vacuum to improve metal-nanotube contacts.<sup>57</sup> Atomic force microscopy (AFM) images were used to exclude multiconnected devices; the remaining individual nanotubes and smaller bundles were used for the present study.<sup>58</sup>

**Functionalization and Defunctionalization.** Functionalization was performed directly onto the devices, using an aqueous reaction of 4-bromobenzenediazonium tetrafluoroborate (BBDT), as described in refs 47 and 44. Sodium hydroxide (NaOH) was dissolved in ultrapure deoxygenated water to obtain a pH of ~9, followed by dissolution of BBDT (2 mM). This high concentration of BBDT was chosen to ensure reproducibility and to prevent selectivity with chirality or diameter.<sup>28,30</sup> Substrates holding nanotube devices were immediately immersed in the BBDT solution for 10 min at room temperature, and then rinsed thoroughly with ultrapure water and diethyl ether. Although graft concentration is difficult to measure directly in individual nanotubes samples, it can be estimated at ~1% of carbon atoms in this study, based on X-ray photoelectron spectroscopy (XPS) measurements and kinetic analysis reported for comparable reactions on bulk samples.<sup>59,60</sup> Defunctionalization was obtained by thermal annealing at 500 °C during 45 min in a vacuum ( $P < 5 \times 10^{-5}$  Torr).<sup>36</sup>

**Electrical Characterization.** Electrical measurements in pristine, functionalized and defunctionalized states were conducted using an ambient probe station, except for temperature-dependent measurements performed in a vacuum probe station (Desert Cryogenic) cooled down using liquid N<sub>2</sub>. In all cases, data was collected using an Agilent B1500A semiconductor parameter analyzer.

**Ab Initio Simulations.** The computational results presented in this article were obtained using the ONETEP simulation software<sup>61</sup> based on density functional theory (DFT).<sup>62,63</sup> Simulation of large system sizes, allowing representation of 4-bromophenyl functionalization of carbon nanotubes, was made possible by the lower and linearly scaling computational work required in this particular implementation of DFT.<sup>64</sup> The simulated systems still have to remain periodic and form a reasonably small primitive cell, which was only possible in the case of armchair (*n,n*) and zigzag (*n,0*) chiralities. In order to model semiconducting nanotubes, zigzag chiralities were selected for the present simulations. The simulated supercell included five nanotube primitive cells (corresponding to an overall length of 2.13 nm), eventually completed by a pair of 4-bromophenyl

groups. Periodic boundary conditions were used to obtain an infinite effective nanotube length, and the choice of including five nanotube primitive cells ensured enough spacing between the periodic replicas of the 4-bromophenyl pair to minimize their interaction. Perpendicular to the nanotube axis, periodic images were separated by at least 3 nm to avoid mutual interaction. Valence wave functions were represented by 1, 4, and 7 Nonorthogonal Generalized Wannier Functions<sup>65</sup> with respective cutoff radii of 7.0, 8.0, and 8.0 bohrs for the H, C and Br atoms. A cutoff energy, alike those of plane wave pseudopotential implementations, was set to a converged value of 35 Ha,<sup>35</sup> and the PBE functional<sup>66</sup> was used throughout all simulations. Finally, geometric optimizations were converged to a precision of 50 meV per supercell, a precision usually unreach-able with traditional linear-scaling DFT implementations.<sup>67</sup>

**Conflict of Interest:** The authors declare no competing financial interest.

**Acknowledgment.** The authors thank B. Simard (NRC) for providing SWNTs and E. Flahaut (U. Toulouse) for DWNTs, as well as P. Haynes (Imperial College London) and N. Hine (University of Cambridge) for their help in the use of ONETEP. This work was made possible by funding from Natural Sciences and Engineering Research Council of Canada (NSERC), and by Calcul Québec and Compute Canada for providing computational resources. D.B. acknowledges the receipt of a Vanier NSERC scholarship, and J.L.J. the receipt of NSERC and FRQNT scholarships.

**Supporting Information Available:** Additional details on numerical simulations, including charge, dispersion and wave function for each graft configuration. This material is available free of charge via the Internet at <http://pubs.acs.org>.

## REFERENCES AND NOTES

- Sze, S. M. *Physics of Semiconductor Devices*; John Wiley & Sons, Inc: New York, 1969.
- Iijima, S. Helical Microtubules of Graphitic Carbon. *Nature* **1991**, *354*, 56–58.
- Han, M.; Özyilmaz, B.; Zhang, Y.; Kim, P. Energy Band-Gap Engineering of Graphene Nanoribbons. *Phys. Rev. Lett.* **2007**, *98*, 206805.
- Morales, A. M.; Lieber, C. M. A Laser Ablation Method for the Synthesis of Crystalline Semiconductor Nanowires. *Science* **1998**, *279*, 208–211.
- Xia, Y.; Yang, P.; Sun, Y.; Wu, Y.; Mayers, B.; Gates, B.; Yin, Y.; Kim, F.; Yan, H. One-Dimensional Nanostructures: Synthesis, Characterization, and Applications. *Adv. Mater.* **2003**, *15*, 353–389.
- Charlier, J.-C. Defects in Carbon Nanotubes. *Acc. Chem. Res.* **2002**, *35*, 1063–1069.
- Collins, P. *Oxford Handb. Nanosci. Technol.* **2010**, 73.
- Xia, Y.; Ma, Y.; Xing, Y.; Mu, Y.; Tan, C.; Mei, L. Growth and Defect Formation of Single-Wall Carbon Nanotubes. *Phys. Rev. B: Condens. Matter Mater. Phys.* **2000**, *61*, 11088–11092.
- Lu, K. L.; Lago, R. M.; Chen, Y. K.; Green, M. L. H.; Harris, P. J. F.; C, T. S. Mechanical Damage of Carbon Nanotubes by Ultrasound. *Carbon* **1996**, *34*, 814–816.
- Krasheninnikov, A.; Nordlund, K.; Sirviö, M.; Salonen, E.; Keinonen, J. Formation of Ion-Irradiation-Induced Atomic-Scale Defects on Walls of Carbon Nanotubes. *Phys. Rev. B: Condens. Matter Mater. Phys.* **2001**, *63*, 245405.
- Gómez-Navarro, C.; de Pablo, P. J.; Gómez-Herrero, J.; Biel, B.; Garcia-Vidal, F. J.; Rubio, A.; Flores, F. Tuning the Conductance of Single-Walled Carbon Nanotubes by Ion Irradiation in the Anderson Localization Regime. *Nat. Mater.* **2005**, *4*, 534–539.

12. Hirsch, A.; Vostrowsky, O. In *Functional Molecular Nanostructures*; Schlüter, A. D., Ed.; Springer: Berlin, 2005; pp 193–237.
13. Tasis, D.; Tagmatarchis, N.; Bianco, A.; Prato, M. Chemistry of Carbon Nanotubes. *Chem. Rev.* **2006**, *106*, 1105–1136.
14. Chen, J.; Hamon, M. A.; Hu, H.; Chen, Y. S.; Rao, A. M.; Eklund, P. C.; Haddon, R. C. Solution Properties of Single-Walled Carbon Nanotubes. *Science* **1998**, *282*, 95–98.
15. Klinke, C.; Hannon, J. B.; Afzali, A.; Avouris, P. Field-Effect Transistors Assembled from Functionalized Carbon Nanotubes. *Nano Lett.* **2006**, *6*, 906–910.
16. Wong, S. S.; Joselevich, E.; Woolley, A. T.; Cheung, C. L.; Lieber, C. M. Covalently Functionalized Nanotubes as Nanometre-Sized Probes in Chemistry and Biology. *Nature* **1998**, *394*, 52–55.
17. Shim, M.; Shi Kam, N. W.; Chen, R. J.; Li, Y.; Dai, H. Functionalization of Carbon Nanotubes for Biocompatibility and Biomolecular Recognition. *Nano Lett.* **2002**, *2*, 285–288.
18. Chen, R. J.; Zhang, Y.; Wang, D.; Dai, H. Noncovalent Sidewall Functionalization of Single-Walled Carbon Nanotubes for Protein Immobilization. *J. Am. Chem. Soc.* **2001**, *123*, 3838–3839.
19. Choi, Y.; Moody, I. S.; Sims, P. C.; Hunt, S. R.; Corso, B. L.; Perez, I.; Weiss, G. A.; Collins, P. G. Single-Molecule Lysozyme Dynamics Monitored by an Electronic Circuit. *Science* **2012**, *335*, 319–324.
20. Chen, Y.; Haddon, R. C.; Fang, S.; Rao, A. M.; Eklund, P. C.; Lee, W. H.; Dickey, E. C.; Grulke, E. A.; Pendergrass, J. C.; Chavan, A.; Haley, B. E.; Smalley, R. E. Chemical Attachment of Organic Functional Groups to Single-walled Carbon Nanotube Material. *J. Mater. Res.* **1998**, *13*, 2423–2431.
21. Pekker, S.; Salvétat, J.-P.; Jakab, E.; Bonard, J.-M.; Forró, L. Hydrogenation of Carbon Nanotubes and Graphite in Liquid Ammonia. *J. Phys. Chem. B* **2001**, *105*, 7938–7943.
22. Nakajima, T.; Kasamatsu, S.; Matsuo, Y. Synthesis and Characterization of Fluorinated Carbon Nanotube. *Eur. J. Solid State Inorg. Chem.* **1996**, *33*, 831–840.
23. Mickelson, E.; Huffman, C.; Rinzler, A.; Smalley, R.; Hauge, R.; Margrave, J. Fluorination of Single-Wall Carbon Nanotubes. *Chem. Phys. Lett.* **1998**, *296*, 188–194.
24. Shaffer, M.; Fan, X.; Windle, A. Dispersion and Packing of Carbon Nanotubes. *Carbon* **1998**, *36*, 1603–1612.
25. Bahr, J. L.; Yang, J.; Kosynkin, D. V.; Bronikowski, M. J.; Smalley, R. E.; Tour, J. M. Functionalization of Carbon Nanotubes by Electrochemical Reduction of Aryl Diazonium Salts: A Bucky Paper Electrode. *J. Am. Chem. Soc.* **2001**, *123*, 6536–6542.
26. Bekyarova, E.; Sarkar, S.; Wang, F.; Itkis, M. E.; Kalinina, I.; Tian, X.; Haddon, R. C. Effect of Covalent Chemistry on the Electronic Structure and Properties of Carbon Nanotubes and Graphene. *Acc. Chem. Res.* **2013**, *46*, 65–76.
27. Bahr, J. L.; Tour, J. M. Covalent Chemistry of Single-Wall Carbon Nanotubes. *J. Mater. Chem.* **2002**, *12*, 1952–1958.
28. An, L.; Fu, Q.; Lu, C.; Liu, J. A Simple Chemical Route to Selectively Eliminate Metallic Carbon Nanotubes in Nanotube Network Devices. *J. Am. Chem. Soc.* **2004**, *126*, 10520–10521.
29. Balasubramanian, K.; Friedrich, M.; Jiang, C.; Fan, Y.; Mews, A.; Burghard, M.; Kern, K. Electrical Transport and Confocal Raman Studies of Electrochemically Modified Individual Carbon Nanotubes. *Adv. Mater.* **2003**, *15*, 1515–1518.
30. Wang, C.; Cao, Q.; Ozel, T.; Gaur, A.; Rogers, J. A.; Shim, M. Electronically Selective Chemical Functionalization of Carbon Nanotubes: Correlation between Raman Spectral and Electrical Responses. *J. Am. Chem. Soc.* **2005**, *127*, 11460–11468.
31. Goldsmith, B. R.; Coroneus, J. G.; Khalap, V. R.; Kane, A. A.; Weiss, G. A.; Collins, P. G. Conductance-Controlled Point Functionalization of Single-Walled Carbon Nanotubes. *Science* **2007**, *315*, 77–81.
32. Strano, M. S.; Dyke, C. A.; Usrey, M. L.; Barone, P. W.; Allen, M. J.; Shan, H.; Kittrell, C.; Hauge, R. H.; Tour, J. M.; Smalley, R. E. Electronic Structure Control of Single-Walled Carbon Nanotube Functionalization. *Science* **2003**, *301*, 1519–1522.
33. Ford, A. C.; Shaughnessy, M.; Wong, B. M.; Kane, A. A.; Kuznetsov, O. V.; Krafcik, K. L.; Billups, W. E.; Hauge, R. H.; Léonard, F. Physical Removal of Metallic Carbon Nanotubes from Nanotube Network Devices Using a Thermal and Fluidic Process. *Nanotechnology* **2013**, *24*, 105202.
34. Darchy, L.; Hanifi, N.; Vialla, F.; Voisin, C.; Bayle, P.-A.; Genovese, L.; Celle, C.; Simonato, J.-P.; Filoramo, A.; Derycke, V.; Chenevier, P. A Highly Selective Non-Radical Diazo Coupling Provides Low Cost Semi-Conducting Carbon Nanotubes. *Carbon* **2014**, *66*, 246–258.
35. Margine, E. R.; Bocquet, M.-L.; Blase, X. Thermal Stability of Graphene and Nanotube Covalent Functionalization. *Nano Lett.* **2008**, *8*, 3315–3319.
36. Cabana, J.; Lavoie, S.; Martel, R. Thermal Chemistry of Methylene- and Phenyl-Functionalized Carbon Nanotubes. *J. Am. Chem. Soc.* **2010**, *132*, 1389–1394.
37. Cabana, J.; Martel, R. Probing the Reversibility of Sidewall Functionalization Using Carbon Nanotube Transistors. *J. Am. Chem. Soc.* **2007**, *129*, 2244–2245.
38. Saito, R.; Dresselhaus, G.; Dresselhaus, M. S. *Physical Properties of Carbon Nanotubes*; Imperial College Press: London, 1998.
39. Lee, Y.-S.; Marzari, N. Cycloaddition Functionalizations to Preserve or Control the Conductance of Carbon Nanotubes. *Phys. Rev. Lett.* **2006**, *97*, 116801.
40. Bouilly, D.; Cabana, J.; Martel, R. Unaltered Electrical Conductance in Single-Walled Carbon Nanotubes Functionalized with Divalent Adducts. *Appl. Phys. Lett.* **2012**, *101*, 053116.
41. Park, H.; Zhao, J.; Lu, J. P. Effects of Sidewall Functionalization on Conducting Properties of Single Wall Carbon Nanotubes. *Nano Lett.* **2006**, *6*, 916–919.
42. López-Bezanilla, A.; Triozon, F.; Latil, S.; Blase, X.; Roche, S. Effect of the Chemical Functionalization on Charge Transport in Carbon Nanotubes at the Mesoscopic Scale. *Nano Lett.* **2009**, *9*, 940–944.
43. Lopez-Bezanilla, A.; Blase, X.; Roche, S. Quantum Transport Properties of Chemically Functionalized Long Semiconducting Carbon Nanotubes. *Nano Res.* **2010**, *3*, 288–295.
44. Bouilly, D.; Cabana, J.; Meunier, F.; Desjardins-Carrière, M.; Lapointe, F.; Gagnon, P.; Larouche, F. L.; Adam, E.; Paillet, M.; Martel, R. Wall-Selective Probing of Double-Walled Carbon Nanotubes Using Covalent Functionalization. *ACS Nano* **2011**, *5*, 4927–4934.
45. Kingston, C. T.; Jakubek, Z. J.; Dénommée, S.; Simard, B. Efficient Laser Synthesis of Single-Walled Carbon Nanotubes through Laser Heating of the Condensing Vaporization Plume. *Carbon* **2004**, *42*, 1657–1664.
46. Flahaut, E.; Bacsá, R.; Peigney, A.; Laurent, C. Gram-Scale CCVD Synthesis of Double-Walled Carbon Nanotubes. *Chem. Commun.* **2003**, 1442–1443.
47. Dyke, C. A.; Tour, J. M. Unbundled and Highly Functionalized Carbon Nanotubes from Aqueous Reactions. *Nano Lett.* **2003**, *3*, 1215–1218.
48. Aguirre, C. M.; Levesque, P. L.; Paillet, M.; Lapointe, F.; St-Antoine, B. C.; Desjardins, P.; Martel, R. The Role of the Oxygen/Water Redox Couple in Suppressing Electron Conduction in Field-Effect Transistors. *Adv. Mater.* **2009**, *21*, 3087–3091.
49. Ong, H. G.; Cheah, J. W.; Zou, X.; Li, B.; Cao, X. H.; Tintang, H.; Li, L.-J.; Zhang, H.; Han, G. C.; Wang, J. Origin of Hysteresis in the Transfer Characteristic of Carbon Nanotube Field Effect Transistor. *J. Phys. D: Appl. Phys.* **2011**, *44*, 285301.
50. Heinze, S.; Tersoff, J.; Martel, R.; Derycke, V.; Appenzeller, J.; Avouris, P. Carbon Nanotubes as Schottky Barrier Transistors. *Phys. Rev. Lett.* **2002**, *89*, 106801.
51. Mott, N. *Conduction in Non-Crystalline Materials*; Oxford University Press: Oxford, 1987; p 128.
52. Transport mechanism analysis is limited by the reduced temperature range available in this experiment, *i.e.*, between the defunctionalization temperature (~600 K) and the temperature at which the low OFF-state current can be detected (>100 K).
53. Zhang, H.; Bekyarova, E.; Huang, J.-W.; Zhao, Z.; Bao, W.; Wang, F.; Haddon, R. C.; Lau, C. N. Aryl Functionalization



- as a Route to Band Gap Engineering in Single Layer Graphene Devices. *Nano Lett.* **2011**, *11*, 4047–4051.
54. Laflamme Janssen, J.; Beaudin, J.; Hine, N. D. M.; Haynes, P. D.; Côté, M. Bromophenyl Functionalization of Carbon Nanotubes: an *Ab Initio* Study. *Nanotechnology* **2013**, *24*, 375702.
  55. Yu, P. Y.; Cardona, M. *Fundamentals of Semiconductors*; Graduate Texts in Physics; Springer: Berlin, 2010; p 775.
  56. Choi, K.; Bourgoïn, J.; Auvray, S.; Esteve, D.; Duesberg, G.; Roth, S.; Burghard, M. Controlled Deposition of Carbon Nanotubes on a Patterned Substrate. *Surf. Sci.* **2000**, *462*, 195–202.
  57. Lee, J.; Park, C.; Kim, J.; Kim, J.; Park, J.; Yoo, K. Formation of Low-Resistance Ohmic Contacts between Carbon Nanotube and Metal Electrodes by a Rapid Thermal Annealing Method. *J. Phys. D: Appl. Phys.* **2000**, *33*, 1953–1956.
  58. Nanotubes forming smaller bundles are expected to react to functionalization similarly as individual nanotubes, unlike large bundles in which inside nanotubes may be protected from functional groups.
  59. Schmidt, G.; Gallon, S.; Esnouf, S.; Bourgoïn, J. P.; Chenevier, P. Mechanism of the Coupling of Diazonium to Single-Walled Carbon Nanotubes and Its Consequences. *Chem.—Eur. J.* **2009**, *15*, 2101–2110.
  60. Fantini, C.; Usrey, M.; Strano, M. Investigation of Electronic and Vibrational Properties of Single-Walled Carbon Nanotubes Functionalized with Diazonium Salts. *J. Phys. Chem. C* **2007**, *111*, 17941–17946.
  61. Skylaris, C.-K.; Haynes, P. D.; Mostofi, A. A.; Payne, M. C. Introducing ONETEP: Linear-Scaling Density Functional Simulations on Parallel Computers. *J. Chem. Phys.* **2005**, *122*, 84119.
  62. Hohenberg, P.; Kohn, W. Inhomogeneous Electron Gas. *Phys. Rev.* **1964**, *136*, 864–871.
  63. Kohn, W.; Sham, L. J. Self-Consistent Equations Including Exchange and Correlation Effects. *Phys. Rev.* **1965**, *140*, 1133–1138.
  64. Hine, N. D. M.; Haynes, P. D.; Mostofi, A. A.; Skylaris, C.-K.; Payne, M. C. Linear-Scaling Density-D Functional Theory with Tens of Thousands of Atoms: Expanding the Scope and Scale of Calculations with ONETEP. *Comput. Phys. Commun.* **2009**, *180*, 1041–1053.
  65. Skylaris, C.-K.; Mostofi, A.; Haynes, P.; Diéguez, O.; Payne, M. Nonorthogonal Generalized Wannier Function Pseudopotential Plane-Wave Method. *Phys. Rev. B: Condens. Matter Mater. Phys.* **2002**, *66*, 035119.
  66. Perdew, J. P.; Burke, K.; Ernzerhof, M. Generalized Gradient Approximation Made Simple. *Phys. Rev. Lett.* **1996**, *77*, 3865–3868.
  67. Hine, N. D. M.; Robinson, M.; Haynes, P. D.; Skylaris, C.-K.; Payne, M. C.; Mostofi, A. A. Accurate Ionic Forces and Geometry Optimization in Linear-Scaling Density-Functional Theory with Local Orbitals. *Phys. Rev. B: Condens. Matter Mater. Phys.* **2011**, *83*, 195102.